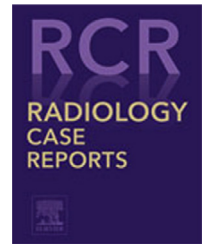


Available online at [www.sciencedirect.com](http://www.sciencedirect.com)

ScienceDirect

journal homepage: [www.elsevier.com/locate/radcr](http://www.elsevier.com/locate/radcr)

## Case Report

# Multiple periapical dysplasias analyzed by cone-beam-computer tomography and <sup>99</sup>Tcm-Scintigraphy. ☆,☆☆,★,★★

Manfred Nilius, MD DDS<sup>a,b,\*</sup>, Minou Nilius, MD<sup>a</sup>, Charlotte Müller, DMD<sup>a</sup>, Henry Leonhardt, MD DMD<sup>b</sup>, Dominik Haim, MD DMD<sup>b</sup>, Patrick Novak, DMD<sup>b</sup>, Adrian Franke<sup>b</sup>, Bernhard Weiland, MD<sup>b</sup>, Guenter Lauer, PhD<sup>b</sup>

<sup>a</sup>Niliusklinik, Dept. of Oral and Maxillofacial Surgery, Dortmund, Germany

<sup>b</sup>Department of Oral and Maxillofacial Surgery, University Hospital "Carl Gustav Carus", Technische Universität Dresden, Dresden, Germany

## ARTICLE INFO

## Article history:

Received 6 July 2021

Revised 22 August 2021

Accepted 25 August 2021

## ABSTRACT

Periapical cemental dysplasia (PCD) is considered a non-neoplastic proliferation of fibrous tissues and cementum-like hard tissues, usually occurring in the periapical regions of teeth. PCD is characterized by the presence of vital pulp and is often accidentally discovered during a general radiographic survey. PCD may arise from the tissue of odontogenic origin or occur as a reactive process in the periapical tissue. Multilocular occurrences in both jaws are rare. However, we encountered a case of multiple PCDs by orthopantomography, which showed different degrees of maturation in the mandible and maxilla by osteodensitometric detection via cone-beam computed tomography (CB-CT) validated by Tc-99m bone-scintigraphy (BS). Biopsies confirmed the radiological results. CB-CT osteodensitometry allows for the categorization and assessment of different stages of PCD maturation from beginning to florid, detection of remittent osseous changes, and evaluation in the clinical follow-up. When using the local cortical bone as a reference value of 100%, periapical dysplasias show density values of 75% in the mandible and 80% in the maxilla. Early classification of PCD is possible with CB-CT osteodensitometry.

☆ Abbreviations: BS, Tc-99m Bone-Scintigraphy; BSgrade, Four categories of Uptake (Tc-99m): No Tc-99m uptake: BSgrade: 0); mild Tc-99m uptake (BSgrade: 1); moderate, Tc-99m uptake (BSgrade: 2); severe Tc-99m uptake, (BSgrade: 3); CB-CT, Cone-beam-computer tomography, CB-CTmat0-4; Categories of periapical remodeling/maturity level; (mat) in CB-CTmat1 (maturity level 1) to CB-CTmat4 (maturity level 4); HU, Hounsfield units; PCD, Periapical cemental dysplasia

☆☆ Competing interests: The authors declare that they have no known competing financial interests or personal relationships that could have appeared to influence the work reported in this paper.

\* Funding: This research did not receive any specific grant from funding agencies in the public, commercial, or not-for-profit sectors.

\*\* Ethics statement: All of the procedures followed were under the ethical standards of the responsible committee on human experimentation (institutional and national) and with the Helsinki Declaration of 1975, as revised in 2008. This article does not contain any studies with human or animal subjects performed by any of the authors.

\* Corresponding author.

E-mail addresses: [manfrednilius@niliusklinik.de](mailto:manfrednilius@niliusklinik.de) (M. Nilius), [bernhard.weiland@uniklinikum-dresden.de](mailto:bernhard.weiland@uniklinikum-dresden.de) (B. Weiland).

<https://doi.org/10.1016/j.radcr.2021.08.067>

1930-0433/© 2021 The Authors. Published by Elsevier Inc. on behalf of University of Washington. This is an open access article under the CC BY-NC-ND license (<http://creativecommons.org/licenses/by-nc-nd/4.0/>)

**Keywords:**  
Disease  
Periapical  
Computed tomographic  
scintigraphy  
Computed tomography  
Cone beam  
Densitometry  
Abnormality  
Jaw  
Cementum  
Dental

© 2021 The Authors. Published by Elsevier Inc. on behalf of University of Washington.  
This is an open access article under the CC BY-NC-ND license  
(<http://creativecommons.org/licenses/by-nc-nd/4.0/>)

## Introduction

Periapical cemental dysplasia (PCD) is a rare benign jaw lesion that originates from a periodontal ligament [1]. In the early stage of its development, it may resemble a periapical lesion. Radiographically, PCD presents with multiple sclerotic masses affecting the cancellous part of the jaws and the tooth-bearing areas in two or more quadrants. Lesions are associated with vital teeth, usually without any clinical sign or complaint, and they are rarely seen in all 4 quadrants [2].

CB-CT is a valuable diagnostic tool, because it can show the axial, sagittal, and frontal sections compared to panoramic radiography [3,4]. In addition, it enables the differentiation of PCD from lesions with a similar sclerotic appearance on conventional radiographs like enostosis or exostosis [5].

Although conventional radiography, which encompasses CB-CT, is more specific, bone scintigraphy is better at detecting early bone changes [6]. BS may be beneficial to diagnosing PCD at an early stage by detecting bone morbidity processes, such as increased bone turnover and new bone formation.

The clinicopathological terminology of PCD lesions has varied over the years and still lacks a consensus [7–9]. Differences in terminology depend on whether the focus is the origin (ie, the undifferentiated cells) or the clinical presentation. According to the classification system introduced by the 1992 Revised World Health Organization (WHO) Guidelines, Periapical Cemento-Osseous Dysplasia is categorized as a form of neoplasm or other bone-related lesions. It can be sub-divided into PCD (also known as Periapical Fibrous Dysplasia), Florid Cemento-Osseous Dysplasia [8,9] (also known as gigantiform cementoma or multiple familial cementoma), and Focal Cemento-Osseous Dysplasia [9]. Some authors discuss familial accumulation in the case of multiple occurrences of these lesions [1,4,11], as reviewed by Nel et al. in 2020 [12].

Regardless of the histopathological classification, these lesions produce differentiable radiological manifestations. For example, in CB-CT, PCD exhibits four degrees of maturation, which produce different radiological images [13].

The first degree of maturation is the osteolytic stage, which is characterized by radiolucent intraosseous ballooning and a thin cortical bone at the apex of the teeth.

In the second degree of maturation, centro-apical sclerosis begins to form radiopaque areas in the radiolucent fields

with the sedimentation of cementum and a sclerotic margin to cancellous bone (edging).

The third degree of maturation presents with sclerotic bone marrow remodeling with distinct radiopacity in many lesions.

In the fourth and final degree of maturation, periapical drumstick formation and hypercementosis are predominant with complete loss of cancellous bone [14–18].

In this study, we describe a case of PCD with different degrees of maturation that affected all four quadrants. To test the efficacy of CB-CT [19] and BS, we compare the results of these two imaging modalities with intraoperative and histopathological findings.

## Case presentation

A 38-year-old woman visited our clinic complaining of a painless swelling of the upper right canine and the lower anterior mandible. She reported that her extremities (arms and legs) grew very quickly when she was in school, and she also reported an early onset of problems with the gum. There was no family history of periodontal diseases. The woman had no siblings. The woman's physique was sporty, her height was 176 cm, and her weight was 64 kg.

Clinical laboratory evaluation, including alkaline phosphatase, parathormone, 25-hydroxy-vitamin D3 (Calcidiol), and fibroblast growth factor 23 [FGF-23], was normal. Beta-Crosslaps (CTX) (124 pg/ml [norm: 150–635]) and osteocalcin 3.78 ng/ml [norm: 8.4–34 ante menopause] were slightly reduced. Genetic analysis did not reveal any evidence of mutations such as Anoctamin-5 or GNAS [20,21].

Intraoral findings: The patient reported the removal of four teeth (tooth numbers 17, 16, 37, and 36) during adult orthodontic treatment. All of the teeth were vital. The patient exhibited mandibular midline shift with right-sided crossbite in regions 12/42 and 22/32 (Fig. 1). Community Periodontal Index of Treatment Needs CPI-TN (WHO) [22]. Grade 2; bleeding on probing (gingival bleeding index according to Ainamo and Bay: GBI: 13% [23]).

Microbiological testing: (Micro-Ident, Hain-Lifescience, Nehren, Germany) Moderate concentration of *Treponema denticola* ( $x < 10^5$ ) and *Tannerella forsythia* ( $x < 10^4$ ); no *Aggregatibacter actinomycetemcomitans*, *Porphyromonas gingivalis*, *Prevotella intermedia*, or other germs were detected. The patient had no history of recent dental extraction/oral surgery, radiotherapy, or chemotherapy.



**Fig. 1** – Intraoral clinical view of a 38-year-old female with multifocal periapical dysplasia.

### Cone-beam CT findings

After initial orthopantomography (Orthophos XG, Sirona Dental Systems, Bensheim, Germany), we performed CB-CT (KaVo 3D eXam ConeBeam XG; KaVo Dental GmbH, Biberach/Riss, Germany) (Fig. 2). We measured the gray values for each apical tooth region [6] and indexed them in Hounsfield units [HU]: 1. the thickest point of the cortical bone, 2. the internal cancellous bone and, if present, 3. the affected apical region with sclerosis (Table 1). We measured sclerotic apical changes. The central starting point of the change was denoted as 'nidus.' We determined the mean values (MEAN) and standard deviation (SD) for the upper jaw and lower jaw from the values of the 3 groups (apical regions indexed as HU 1, 2, and 3) and presented them graphically (Excel, version 2014, Microsoft 365). We compared the CB-CT results of the three groups and assigned each group to a degree of maturation according to the clinical-radiological categories of maturation of periapi-

cal dysplasias [2] (Table 2). We added a fourth category for changes in the edentulous regions [2,25]. We made a diagnosis via BS and CB-CT to exclude aggressive bone lesions [6] and calculated the correlation of the findings (Table 3) [26]. We performed extirpation of pulp 13, harvested bony biopsies in apical region 13, and obtained a specimen from pre-implant augmentation region 036 to verify nuclear medicine and radiological findings.

### Tc-99m bone-scintigraphy (BS)

We performed radionuclide BS 2 h after IV injection of technetium-99m methylene diphosphonate (Tc-99m MDP; 520.0 MBq after 2 h; pixel size 2.1, SL 1880; SP 4.2 mm/s) in anteroposterior (AP) (Fig. 3A) and lateral (LAT) projections (Fig. 3B) [6,26]. To finally confirm radiological findings, we conducted histopathology of surgical specimens of bone destruction. The patient provided informed consent for investigation with a technetium bone scan.

## Results

Periapical regions of all of the teeth had radiological findings. Apically, the upper right canine had an approximately 10 mm × 10 mm hyperdense structure surrounding the apex, breaking through the cortex, and filling the medullary canal. The apex from tooth 12 had a comparable finding. Apices 21 and 22 had an approximately 9 mm × 8 mm irregular structure with hyperdense central nidus-like signs of sclerosis in a confluent, hypodense environment. This structure distorted the vestibular compacta. Apex 22 had a comparable finding.

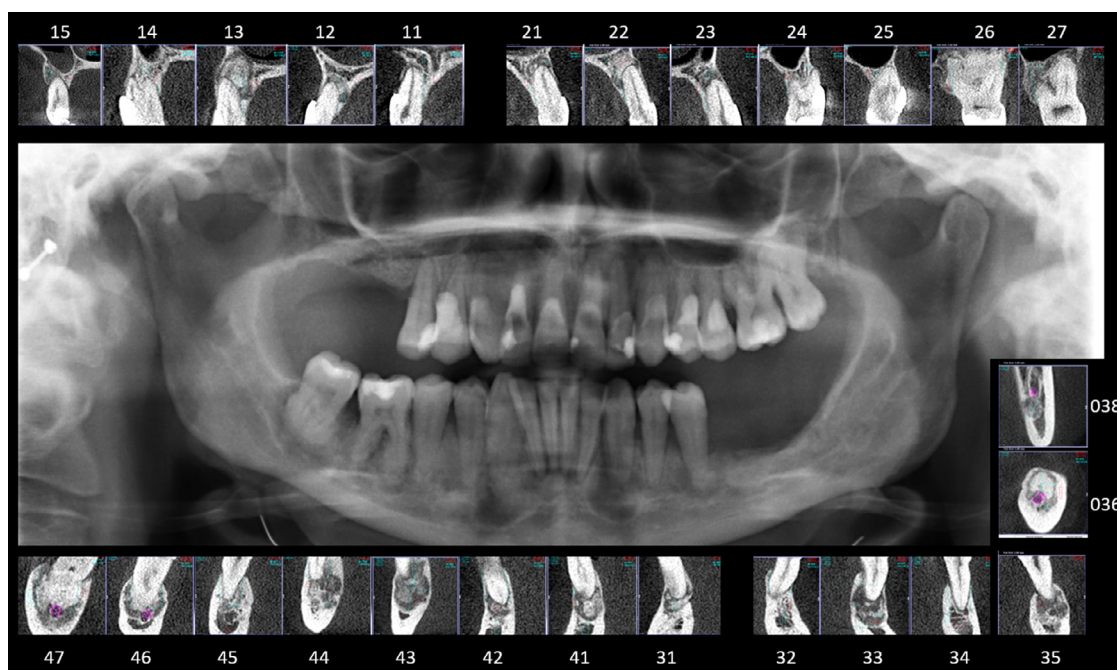


**Fig. 2** – Center: orthopantomography; frame: cross-sectional images in the sagittal dimension from CB-CT for each periapical region.

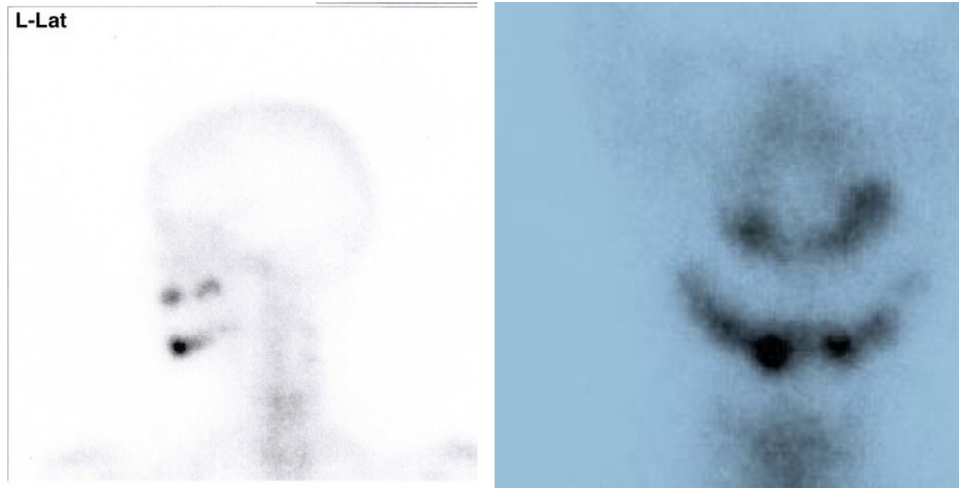


**Fig. 3 – Tc-99m bone scintigraphy (BS) of the head in anteroposterior (A) and lateral left (B) projection 2 h after IV injection of technetium-99m methylene diphosphonate (Tc-99m MDP; 520.0 MBq after 2 h; pixel size 2.1, SL 1880; SP 4.2 mm/s).**

Apical 26/27 had a hyperdense area of approximately 16 mm × 15 mm filling the medullary canal.

In region 038, at the junction of the horizontal and ascending mandible, there was an approximately 5 mm osteolysis of the lingual bony cortex. In the left jaw angle, in caudal con-

tact with the mandibular canal, there was an approximately 6.5 mm round, inhomogeneous, partly intracortical hypodensity with a discrete protrusion of the lingual compacts. In region 036/037, there was an approximately 11 mm × 5 mm long, sharply demarcated calcification-like structure within

**Table 1 – Grayscale [HU] for different maxillary and mandibular bone regions: cortical mandible [blue]; cortical maxilla [red]; nidus mandible [gray]; nidus maxilla [orange]; cancellous maxilla [dark blue]; and cancellous mandible [green].**

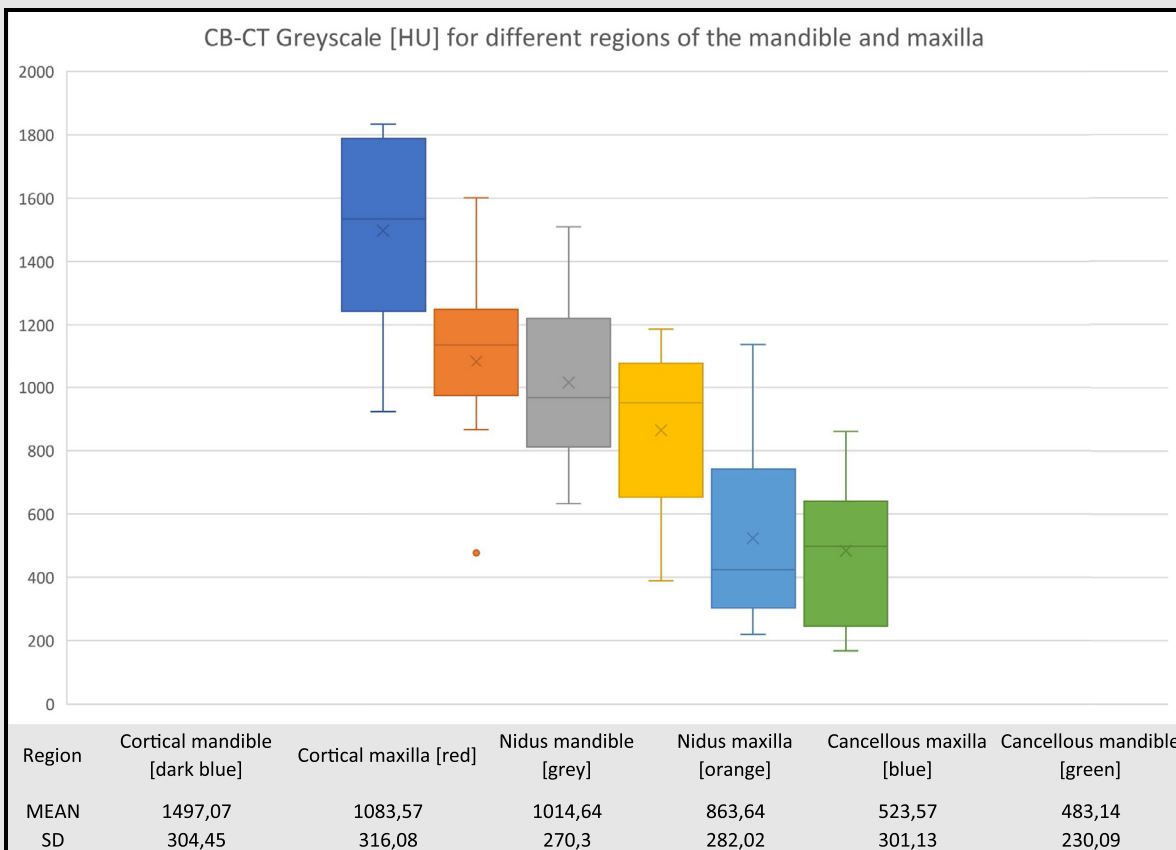


**Table 2 – Periapical density [HU] from the CB-CT for different lower and upper jaw areas (tooth/area). We evaluated the density of cortical and cancellous bone and central sclerosis (nidus). The density values were assigned the degree of maturation, Tc-99m uptake, sclerotic margin, erosion of the compacta, and drumstick formation/hypercementosis.**

| Tooth/Area | Cortical HU [MEAN] | Cancellous HU [MEAN] | Central sclerosis (Nidus) HU [Mean] | Category of maturation | Scintigraphic Uptake | Sclerotic rim | Arosion of compacta | Drumstick/Hypercementosis |
|------------|--------------------|----------------------|-------------------------------------|------------------------|----------------------|---------------|---------------------|---------------------------|
| 17         | 477                | 389                  | 389                                 | 0                      | 0                    | --            | --                  | --                        |
| 16         | 477                | 389                  | 389                                 | 0                      | 0                    | --            | --                  | --                        |
| 15         | 1177               | 370                  | 700                                 | 1                      | 0                    | --            | --                  | --                        |
| 14         | 1199               | 1060                 | 1060                                | 3                      | 1                    | --            | --                  | --                        |
| 13         | 1010               | 460                  | 1020                                | 3                      | 2                    | Yes           | Yes                 | --                        |
| 12         | 1010               | 330                  | 1060                                | 2                      | 1                    | Yes           | Yes                 | --                        |
| 11         | 1601               | 220                  | 1010                                | 1                      | 0                    | Yes           | --                  | --                        |
| 21         | 1405               | 467                  | 892                                 | 1                      | 1                    | Yes           | Yes                 | --                        |
| 22         | 1145               | 223                  | 1186                                | 2                      | 1                    | Yes           | Yes                 | --                        |
| 23         | 1132               | 510                  | 510                                 | 1                      | 1                    | --            | --                  | --                        |
| 24         | 1135               | 843                  | 843                                 | 0                      | 0                    | --            | --                  | --                        |
| 25         | 865                | 708                  | 708                                 | 0                      | 0                    | --            | --                  | --                        |
| 26         | 1138               | 1138                 | 1138                                | 3                      | 2                    | Yes           | --                  | D                         |
| 27         | 1399               | 223                  | 1186                                | 3                      | 2                    | Yes           | --                  | D                         |
| 38         | 1731               | 635                  | 810                                 | 2                      | 1                    | Yes           | Yes                 | --                        |
| 37         | 1833               | 860                  | 1509                                | 4                      | 1                    | Yes           | Yes                 | H                         |
| 36         | 1833               | 784                  | 1509                                | 4                      | 1                    | Yes           | Yes                 | H                         |
| 35         | 1479               | 636                  | 1219                                | 2                      | 1                    | Yes           | Yes                 | --                        |
| 34         | 1589               | 632                  | 632                                 | 1                      | 2                    | --            | --                  | --                        |
| 33         | 1452               | 497                  | 968                                 | 2                      | 3                    | Yes           | Yes                 | --                        |
| 32         | 1633               | 490                  | 1059                                | 1                      | 2                    | Yes           | --                  | --                        |
| 31         | 1232               | 497                  | 983                                 | 2                      | 1                    | Yes           | Yes                 | --                        |
| 41         | 1189               | 252                  | 782                                 | 2                      | 1                    | Yes           | Yes                 | --                        |
| 42         | 923                | 227                  | 821                                 | 2                      | 2                    | Yes           | Yes                 | --                        |
| 43         | 1131               | 185                  | 965                                 | 2                      | 3                    | Yes           | Yes                 | --                        |
| 44         | 1275               | 632                  | 1224                                | 2                      | 3                    | --            | Yes                 | --                        |
| 45         | 1797               | 168                  | 922                                 | 2                      | 2                    | Yes           | Yes                 | --                        |
| 46         | 1833               | 254                  | 671                                 | 3                      | 1                    | Yes           | Yes                 | --                        |
| 47         | 1760               | 650                  | 941                                 | 3                      | 1                    | Yes           | Yes                 | D                         |

the cancellous bone, partly confluent with apical regions 35–33. Similar findings were obtained in regions 41 and 43–47. There was no perforation of the vestibular cortex 43. On tooth 47, there was a roundish, well-delimited cystic change with a diameter of approximately 20 mm and sclerosis of the edge area, beginning at the coronal collar junction and reaching the mandibular canal. We found a drumstick formation, also called a ginger root formation, only in the molar regions.

The density values of the apical lesions show, on average, lower values than the local cortical bone, regardless of whether it is the maxilla or the mandibula. The differences are more evident in the lower jaw ([HU] cortical MEAN 1497.07/SD: 304.45); nidus mandible (MEAN 1083.57/SD 316.08) than in the upper jaw (cortical MEAN 1083.57/SD 316.08; nidus maxilla MEAN 863.64/SD: 282); this could serve as a guideline for comparative intra-individual examinations. The nidus value is, on average, 75% of the cortical density value for the upper jaw; and it is around 80% of the initial cortical value for the mandible.

We identified several areas in the upper jaw and the mandible with nuclide enrichment in the scintigraphy, and we decided to separate them into four groups based on intensity:

No Tc-99m uptake (BSgrade: 0);

1: mild Tc-99m uptake (BSgrade: 1);

2: moderate Tc-99m uptake (BSgrade: 2);

3: severe Tc-99m uptake (BSgrade: 3). The categories were summarized and compared to the CB-CT-findings in (Table 2).

Based on the categories of maturation [2] and Tc-99m uptake, we found the following densities in CB-CT:

CB-CTmat1 (Maturity level 1): intraosseous ballooning, thinning of the cortical bone [HU: MEAN 915; SD: 160]; beginning accumulation on Tc-99m scintigraphy (BSgrade: 1).

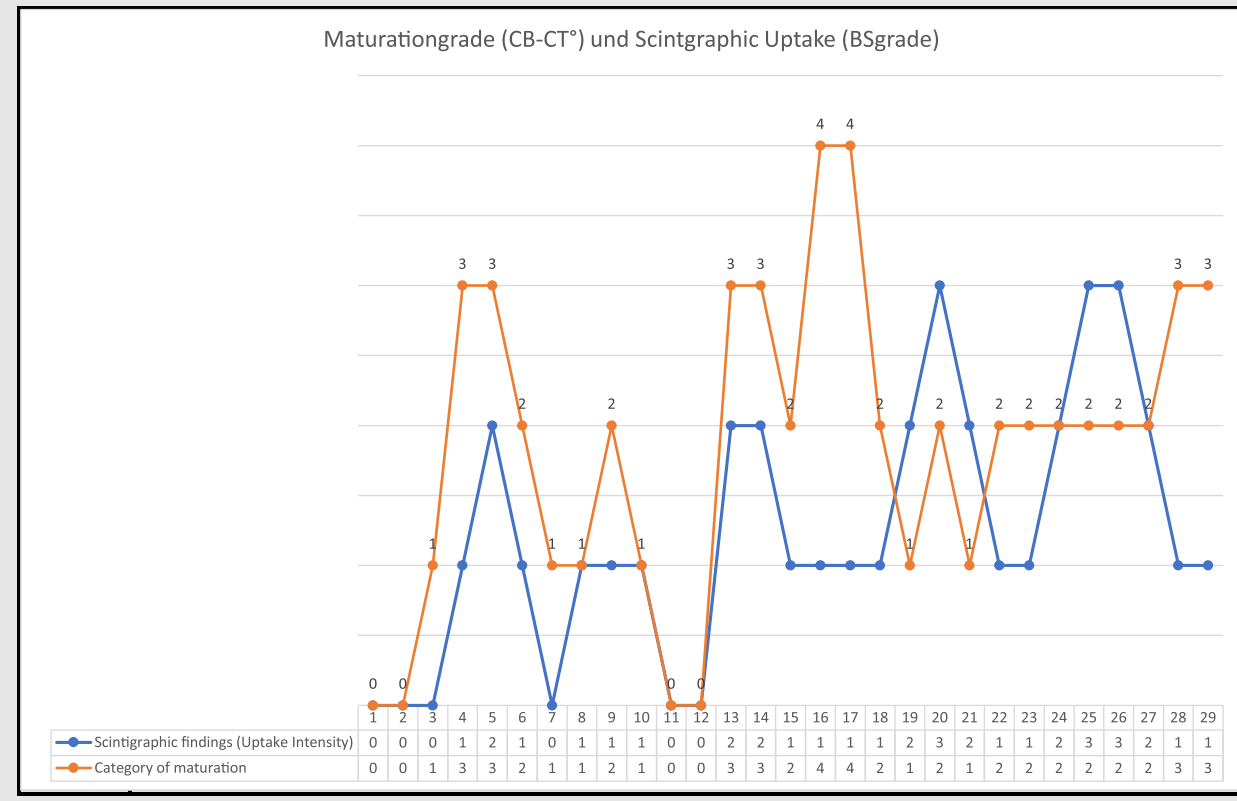
CB-CTmat2 (Maturity level 2): apico-central sclerosis, sclerotic margin (edging) to cancellous bone [HU: MEAN 995; SD: 161]; increasing accumulation on Tc-99m scintigraphy (BSgrade: 2).

CB-CTmat3 (Maturity level 3): sclerotic remodeling of the bone marrow [HU: MEAN 1003; SD: 184]; intense accumulation on Tc-99m scintigraphy (BSgrade: 3).

CB-CTmat4 (Maturity level 4): periapical drumstick formation (ginger root), hypercementosis [HU: MEAN 1059; SD: 0]; decreasing accumulation on Tc-99m scintigraphy (BSgrade: 1–2).

The regions of the molars showed the most advanced categories of maturation (CB-CTmat3 and 4). In the lower jaw,

**Table 3 – Maturity level (CB-CTmat) and scintigraphic uptake (BSgrade) for each tooth area.**



there were residuals in regions 038–036, with sclerosing filling the medullary canal (CB-CTmat4; BSgrade: 1). On the contrary, all of the front teeth showed progressive remodeling processes (CB-CTmat2/BSgrade: 2). In addition, the right lower premolar and the right upper canine with category three maturation were in the stage of florid sclerosis (CB-CTmat3; BSgrade: 3) visible through pronounced nuclide accumulation in the scintigraphy.

**Discussion**

**Periapical dysplasia**

Most researchers do not see cement hyperplasia as a natural tumor but rather as a reactive occurrence. The only disputed issue is whether the reaction arises from odontogenic tissue or periapical bone. In addition, trauma, infections, or hormonal changes may [10] play an etiological role [9,10,27]. Cement hyperplasia differs from hypercementosis in its localized occurrence and its gradual course [28]. Cement-osseous dysplasia (COD) is widespread in women around the age of 40 [12]. Most commonly, apical cement dysplasia occurs on the lower anterior teeth. Usually, there are multiple occurrences in familial florid cemento-osseous dysplasia [11]. We did not identify familiar accumulation in this case. As a rule, there are no symptoms associated with the disease un-

less the N. mentalis is irritated. Macroscopically, the cement dysplasia of the root tip is cap-shaped. Thus, different appearances in the X-ray can be distinguished. We have represented these differences with Hounsfield Units (HU) through the three-dimensional CB-CT. In CB-CTmat1, periapical fibrosis with the destruction of the bone is visible. In the X-ray image, this is shown in a rounded focal point.

Additionally, in CB-CT, there is intraosseous ballooning and thinning of the cortical rim. The central nidus [HU: MEAN 915; SD: 160] correlates to a mild scintigraphic uptake of radionuclides (BSgrade: 1). In terms of differential diagnosis, the differentiation from apical granuloma can be ruled out by vitality testing because the tooth remains vital in cement dysplasia. In CB-CTmat2, cementoblastic maturation begins. Cement formation typically occurs in the central parts of the lesion, so lime-thick shadows appear within the foci of lightning in the X-ray image. At this stage, the X-ray is typical and distinctive. CB-CTmat2 shows surplus edging of a sclerotic margin to cancellous bone [HU: MEAN 995; SD: 161]. This grade presents a strong nuclide-uptake in scintigraphy (BSgrade: 3), and mineralization moves forward.

CB-CTmat3 is characterized by excessive deposits of radiopaque cement and commonly marks the final stage of periapical dysplasia [2,11,24]. However, there is always a narrow halo of a brightening zone around the radiopaque shadows. In CB-CTmat3, sclerotic remodeling of the bone marrow and CB-CT grayscale increases [HU: MEAN 1003; SD: 184]; scintigraphic uptake is moderate (BSgrade 2).

CB-CTmat4 is characterized by periapical formation without the halo of the brightening zone and bridging of periodontal space. Radiologically, it appears similar to hypercementosis [HU: MEAN 1059; SD: 0]. The scintigraphic grade is 1 (BSgrade: 1) since uptake is less than previous stages or impacted teeth. Macroscopically, hypercementosis appears locally at the tip of the root or diffusely over the entire surface of the root. Clinical complaints are rare. There is a piston-shaped widening of the tooth root with thickening and clumping. The root tip is round and plump like a drumstick or ginger root. Microscopically, irregular cement in different layers, like tree bark, lies over the narrow edge of the usual cement. This cement differs in its cellularity, hence the name "cellular cement." Because of its similarity to bone, Minderjan uses the term "osteocement." [2]. Pathogenetically, it is considered a post-inflammatory entity. In this study, only the molars had the upper left side and the lower right side could be examined, as the molars have already been removed in the other two quadrants. Since there were only the upper left and lower right molars in place, we hypothesize that inflammation or trauma starts in the distal parts of the jaws and matures with sclerosis. In this case, these teeth showed no sign of movement or infection. Horizontal bone loss, orthodontic treatment, or periodontal superinfection may cause tooth loss in the other molar regions. Like PCD, hypercementosis mainly occurs at the tip of the root. However, once healed, clinical and radiological delimitation can be difficult. Localized deposits of cellular root cement lead to drumstick-like changes in the apex and bridge the apical periodontal gap. Lesions nearby may coalesce to form larger sclerotic zones (regions 036–037). From the authors' point of view, hypercementosis (or formation of "ginger-roots") may be regarded as the fourth stage in the maturation of PCD. A tumorous variation of cement dysplasia is the central cement-forming fibroma, preferentially on the lower jaw in young adults. Histological findings correspond to those of cement dysplasia. Therefore, we excluded this tumor originating from the tissue's connective tissue cells by biopsy [9,27–29].

Fibrous dysplasia was excluded by testing GNAS negative. We investigated hyperparathyroidism-jaw tumor syndrome (HPT-JT) and gnathodiaphyseal dysplasia (GDD) as potential diagnoses. Hyperparathyroidism-jaw tumor syndrome is a genetic condition associated with hyperparathyroidism, multiple parathyroid adenomas, renal tumors, and multiple ossifying fibromas [30–32]. We excluded all of these diagnoses since the PCD patients do not typically present bone-associated comorbidities. However, we excluded the diagnosis of GDD because our patient had no history of long bone fractures as described by [33].

The differentiation of pathological processes with bone involvement is a central task of radiological diagnostics. CB-CT offers some advantages in categorizing benign and malignant jaw tumors [6,30,34]. In addition, CB-CT can be used to assess fine bone structure for dental implantology and delimit primarily inflammatory destructive processes (such as osteomyelitis, differentiation of complications after therapeutic interventions, and infections). The main advantages of CB-CT are lower costs, low susceptibility to artifacts, radiological dose reduction by half compared to CT, and spatial resolution comparable to CT.

We used osteodensitometry to determine the bone density and thus the bone quantity in periapical dysplasias. Lytic and remineralizing processes take place parallel to the inflammatory bone. Therefore, osteodensitometry helps determine bone healing (maturation), as in the case of multilocular periapical dysplasia. Conventional X-rays are unsuitable for this, as they only show mineral salt losses from around 30% of the norm. Instead, we used Tc99 scintigraphy to detect inflammatory processes through the accumulation of Tc99 in high-turnover tissues [6]. Therefore, Tc99 scintigraphy can be used to indicate the severity of the inflammation and prove CB-CT findings. However, the method is not precise due to the pixel size.

### CB-CT osteodensitometry

The density measurement of CT—the grayscale—is based on the Hounsfield scale as a function of the attenuation value of water. As expected, the calibration curves of CTs follow a linear increase. According to Bhagwat et al. 2010 [34] and Li et al. 2019 [35], CB-CT calibration curves also follow a linear increase. However, the slope of the curves of CT and CB-CT can vary, so a conversion factor of the density values should be determined to compare findings from CT and CB-CT. Irrespective of the device-specific correction factor, intra-individual maturity levels can be determined through differences in density.

A device-specific correlation coefficient is necessary to calculate the actual Hounsfield unit to include former CT-based examinations for follow-up or retrospective analyses to compare CT with CB-CT.

---

## Conclusion

This investigation shows that CB-CT can be used for bone density measurement of pathological processes such as periapical dysplasia. Calculating differences in Hounsfield Units (HU) via CB-CT osteodensitometry allows for the categorization of PCD maturity and supporting clinical monitoring. We used the density of the cortical bone as an intra-individual guide value. Thus, a clear assignment of periapical dysplasia can be made based on the nidus density, the nidus extent, and the radiological morphology. The nidus value is on average 75% of the cortical density value for the upper jaw and around 80% of the initial cortical value for the mandible. Of course, this ratio should be checked individually, but it could serve as a guideline for comparative intra-individual examinations.

Quantitative determination of bone density through dental CB-CT could also be applied to automated screening analysis by implementing diagnostic programs with the help of artificial intelligence.

---

## Patient consent

The patient gave written consent for publication. The author should ensure that the work described has been

carried out following The Code of Ethics of the World Medical Association (Declaration of Helsinki). Furthermore, the manuscript should be in line with the Recommendations for the Conduct, Reporting, Editing, and Publication of Scholarly Work in Medical Journals and aim to include representative human populations (sex, age, and ethnicity) as per those recommendations.

All of the authors contributed to the study's conception and design, commented on previous versions of the manuscript, and read and approved the final manuscript.

## REFERENCES

- [1] Falace D, Cunningham C. Periapical cemental dysplasia: simultaneous occurrence in multiple maxillary and mandibular teeth. *J Endod* 1984;10:455–6. doi:10.1016/S0099-2399(84)80269-1.
- [2] Minderjahn A. Incidence and clinical differentiation of odontogenic tumours. *J Maxillofac Surg* 1979;7:142–50. doi:10.1016/s0301-0503(79)80027-2.
- [3] Scarfe WC, Farman AG. What is cone-beam CT and how does it work? *Dent Clin N Am* 2008;52:707–30. doi:10.1016/j.cden.2008.05.005.
- [4] Chennoju SK, Pachigolla R, Govada VM, Alapati S, Balla S. Idiosyncratic presentation of cemento-osseous dysplasia - an in depth analysis using cone beam computed tomography. *J Clin Diagn Res* 2016;10:ZD08–10. doi:10.7860/JCDR/2016/16821.7839.
- [5] Bhandari R, Sandhu SV, Bansal H, Behl R, Bhullar RK. Focal cemento-osseous dysplasia masquerading as a residual cyst. *Contemp Clin Dent* 2012;3:S60. doi:10.4103/0976-237X.95107.
- [6] Jamdade A, John A. Bone scintigraphy and panoramic radiography in deciding the extent of bone resection in benign jaw lesions. *J Clin Diagn Res* 2013;7:2351–5. doi:10.7860/JCDR/2013/5963.3522.
- [7] Beylouni I, Farge P, Mazoyer JF, Coudert JL. Florid cemento-osseous dysplasia: report of a case documented with computed tomography and 3D imaging. *Oral Surg Oral Med Oral Pathol Oral Radiol Endod* 1998;85:707–11. doi:10.1016/s1079-2104(98)90039-7.
- [8] Kramer IR, Pindborg JJ, Shear M. The WHO histological typing of odontogenic tumours. a commentary on the second edition. *Cancer* 1992;70:2988–94. doi:10.1016/0964-1955(93)90018-a.
- [9] MacDonald- Jankowski DS. Florid cemento- osseous dysplasia: a systematic review. *Dentomaxillofac Radiol* 2003;32:141–9. doi:10.1259/dmfr/32988764.
- [10] Roghi M, Scapparone C, Crippa R, Silvestrini-Biavati A, Angiero F. Periapical cemento-osseous dysplasia: clinicopathological features. *Anticancer Res* 2014;34:2533–6.
- [11] Thakkar NS, Horner K, Sloan P. Familial occurrence of periapical cemental dysplasia. *Virchows Arch A Pathol Anat Histopathol* 1993;423:233–6. doi:10.1007/BF01614776.
- [12] Nel C, Yakoob Z, Schouwstra CM, van Heerden W, et al. Familial florid cemento-osseous dysplasia: a report of three cases and review of the literature. *Dentomaxillofac Radiol* 2021;50:20190486. doi:10.1259/dmfr.20190486.
- [13] Komabayashi T, Zhu Q. Cemento-osseous dysplasia in an elderly asian male: a case report. *J Oral Sci* 2011;53:117–20. doi:10.2334/josnusd.53.117.
- [14] Summerlin DJ, Tomich CE. Focal cemento-osseous dysplasia: a clinicopathologic study of 221 cases. *Oral Surg Oral Med Oral Pathol* 1994;78:611–20. doi:10.1016/0030-4220(94)90174-0.
- [15] Scholl RJ, Kellett HM, Neumann DP, Lurie AG. Radiographics. cysts and cystic lesions of the mandible: clinical and radiologic-histopathologic review. *Radiographics* 1999;19:1107–24. doi:10.1148/radiographics.19.5.g99se021107.
- [16] Arijji Y, Arijji E, Higuchi Y, Kubo S, Nakayama E, Kanda S. Florid cemento-osseous dysplasia. radiographic study with special emphasis on computed tomography. *Oral Surg Oral Med Oral Pathol* 1994;78:391–6. doi:10.1016/0030-4220(94)90074-4.
- [17] Kutluay Köklü H, Cankal DA, Bozkaya S, Ergün G, Bar E. Florid cemento-osseous dysplasia: report of a case documented with clinical, radiographic, biochemical and histological findings. *J Clin Exp Dent* 2013;5(1):e58–61. doi:10.4317/jced.50854.
- [18] Brody A, Zaltnai A, Csomo K, Belik A, Dobo-Nagy C. Difficulties in the diagnosis of periapical translucencies and in the classification of cemento-osseous dysplasia. *BMC Oral Health* 2019;19:139. doi:10.1186/s12903-019-0843-0.
- [19] Shibata N, Inamoto K, Naitoh M, Arijji E. Clinical assessment of cemento-osseous dysplasia based on 3-dimensional diagnostic imaging: a case report. *Aust Endod J* 2021;47:105–12. doi:10.1111/aej.12488.
- [20] Riminucci M, Collins MT, Corsi A, et al. Gnathodiaphyseal dysplasia: a syndrome of fibro-osseous lesions of jawbones, bone fragility, and long bone bowing. *J Bone Miner Res* 2001;16:1710–18. doi:10.1359/jbmr.2001.16.9.1710.
- [21] Wang X, Liu X, Dong R, Liang C, Reichenberger EJ, Hu Y. Genetic disruption of anoctamin 5 in mice replicates human gnathodiaphyseal dysplasia (GDD). *Calcif Tissue Int* 2019;104:679–89. doi:10.1007/s00223-019-00528-x.
- [22] Ainamo J, Barmes D, Beagrie G, Cutress T, Martin J, Sardo-Infirri J. Development of the World Health Organization (WHO) community periodontal index of treatment needs (CPITN). *Int Dent J* 1982;32:281–91.
- [23] Ainamo J, Bay I. Problems and proposals for recording gingivitis and plaque. *Int Dent J* 1975;25:229–35.
- [24] Raubenheimer EJ, Noffke CE, Boy SC. Osseous dysplasia with gross jaw expansion: a review of 18 lesions. *Head Neck Pathol* 2016;10:437–43. doi:10.1007/s12105-016-0720-y.
- [25] Warriar SA, Vinayachandran D. Irregular periapical radiopacity in mandibular premolars and molars. *Case Rep Dent* 2014;Epub 2014 Feb 20(2014:910843):910843. doi:10.1155/2014/910843.
- [26] Taki S, Tonami N, Taki J, Muroki T, Yamamoto E, Hisada K. Intense accumulation of Tc-99m MDP and Ga-67 in multiple periapical cemental dysplasia. *Ann Nucl Med* 1995;9:243–5. doi:10.1007/BF03168408.
- [27] Speight PM, Carlos R. Maxillofacial fibro- osseous lesions. *Curr Diagn Pathol* 2006;12:1–10. doi:10.1016/j.cdip.2005.10.002.
- [28] Sim YC, Bakhshalian N, Lee J- H, Ahn K-M. Familial florid cemento- osseous dysplasia in mother and her identical twins: a report with review of the literatures. *Oral Surgery* 2014;7:239–44. doi:10.1111/ors.12082.
- [29] de Noronha Santos Netto J, Cerri JM, Miranda ÁMMA, Pires FR. Benign fibro- osseous lesions: clinicopathologic features from 143 cases diagnosed in an oral diagnosis setting. *Oral Surg Oral Med Oral Pathol Oral Radiol* 2013;115:e56–65. doi:10.1016/j.oooo.2012.05.022.
- [30] El-Mofty SK. Fibro- Osseous lesions of the craniofacial skeleton: an update. *Head Neck Pathol* 2014;8:432–44. doi:10.1007/s12105-014-0590-0.
- [31] du Preez H, Adams A, Richards P, Whitley S. Hyperparathyroidism jaw tumor syndrome: a pictorial review. *Insights Imaging* 2016;7:793–800. doi:10.1007/s13244-016-0519-0.

- 
- [32] Hobbs MR, Pole AR, Pidwirny G, Rosen I B, Zarbo R J, Coon H, et al. Hyperparathyroidism-jaw tumor syndrome: the HRPT2 locus is within a 0.7-cM region on chromosome 1q. *Am J Hum Genet* 1999;64:518–25. doi:[10.1086/302259](https://doi.org/10.1086/302259).
- [33] Duong HA, Le KT, Soulema AL, Youh RH, Scheuner MT, Holick MF, et al. Gnathodiaphyseal dysplasia: report of a family with a novel mutation of the ANO5 gene. *Oral Surg Oral Med Oral Pathol Oral Radiol* 2016;121:e123–8. doi:[10.1016/j.oooo.2016.01.014](https://doi.org/10.1016/j.oooo.2016.01.014).
- [34] Bhagwat MS, Blessing M, Lyatskaya Y, Zygmanski P. A phenomenological kV beam model for cone-beam imaging. *Phys Med Biol* 2010;55:5787–99. doi:[10.1088/0031-9155/55/19/011](https://doi.org/10.1088/0031-9155/55/19/011).
- [35] Li G, Luo S, You C, Getzin M, Zheng L, Wang G, et al. A novel calibration method incorporating nonlinear optimization and ball-bearing markers for cone-beam CT with a parameterized trajectory. *Med Phys* 2019;46:152–64. doi:[10.1002/mp.13278](https://doi.org/10.1002/mp.13278).